Slow convergence in viscous lens coalescence

Walter Tewes[1]†, Charu Datt[1]‡, Michiel A. Hack[1]‡ and Jacco H. Snoeijer[1]

[1]Physics of Fluids Group, Faculty of Science and Technology, University of Twente, P.O. Box 217, 7500 AE Enschede, The Netherlands

(Received xx; revised xx; accepted xx)

Drop coalescence occurs through the rapid growth of a bridge that connects the two drops. At early times after contact the bridge dynamics is typically self-similar, with details depending on the geometry and viscosity of the liquid. In this paper we analyse the coalescence of viscous drops that float on a quiescent deep pool; such drops are called liquid lenses. The analysis is based on the thin-sheet equations, which were recently shown to accurately capture experiments of liquid lens coalescence. We find that the speed of visco-capillary coalescence is not constant, but exhibits a slow logarithmic evolution with time. This dynamics is explained using a matched asymptotic expansion, which reveals a slow evolution of quasi-self-similar flow profiles. The analysis predicts that the coalescence velocity exhibits a weak dependence on the ratio of the bridge height and drop size, as is confirmed in detail by numerical simulations.

1. Introduction

Coalescence of drops is one of the most common capillarity-driven phenomena which can be observed in multiphase fluid dynamics. The early-time dynamics of coalescence is dependent on both the viscosity of the drops and their geometry. Different power laws for the growth of the connecting structure (referred to as *neck* or *bridge*) have been found for viscous and inviscid freely suspended drops (Eggers *et al.* 1999; Duchemin *et al.* 2003; Thoroddsen *et al.* 2007; Paulsen *et al.* 2011; Aarts *et al.* 2005), as well as for sessile drops in the viscous and inviscid limit (Ristenpart *et al.* 2006; Hernández-Sánchez *et al.* 2012; Eddi *et al.* 2013; Narge *et al.* 2008; Lee *et al.* 2012). The study of coalescence phenomena is also relevant for many applications where the underlying substrate of the coalescing drops is a liquid. Some examples are wet-on-wet printing (Hack *et al.* 2018), emulsions (Shaw 2003; Kamp *et al.* 2016), and lubricant impregnated substrates (Smith *et al.* 2013; Anand *et al.* 2012).

Here, we focus on liquid lenses (de Gennes *et al.* 2004), consisting of liquid drops floating on a quiescent pool of another liquid. This case was studied for Newtonian drops (Burton & Taborek 2007) and liquid crystals (Delabre & Cazabat 2010), where the authors analysed the growth of the bridge in top-view experiments. Recent work considered the coalescence of lenses using side-view experiments (Hack *et al.* 2020). This perspective is sketched in figure 1, providing a quasi-two-dimensional view of the problem. The experiments revealed a self-similar dynamics of the bridge profiles, with scaling laws for the bridge height h_0 that depend on the viscosity (Hack *et al.* 2020). At low viscosity, the dominant balance during coalescence is between surface tension and inertia, and it was found that $h_0 \sim t^{2/3}$. At high viscosity, the dominant balance between surface tension and viscosity leads to $h_0 = V_0 t$ where V_0 is the coalescence velocity. These

‡ C. Datt and M. A. Hack contributed equally to this work.
† Email address for correspondence: w.b.h.tewes@utwente.nl

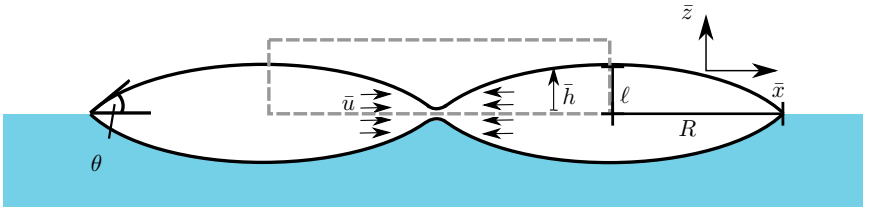

FIGURE 1. Sketch of two coalescing lenses of height ℓ, radius R and equilibrium contact angle θ. The dashed rectangle shows the domain considered in the modeling.

scaling laws are the same as those described in the merging of liquid wedges (Billingham & King 2005). Owing to the slender geometry of the drops – typically the contact angle θ in figure 1 is small – the coalescence of liquid lenses can be analysed using the thin-sheet equations (Erneux & Davis 1993; Ting & Keller 1990). Using a similarity analysis, the experimentally observed inertial and viscous scaling laws are recovered (Hack *et al.* 2020). For example, the viscous coalescence speed was found $V_0 = 2.21..\frac{\gamma\theta^2}{4\eta}$, where γ and η respectively are the drop surface tension and viscosity, in good agreement with experiments.

Interestingly, the viscous similarity analysis contains an important inconsistency: the obtained self-similar velocity profile does not decay at large distance from the thin bridge region. This is problematic, since in coalescence (as well as in drop breakup, cf. Eggers & Fontelos (2015)), the similarity analysis is based on the assumption that the flow remains confined to the scale of the neck – at large scale, i.e. the scale of the drop, the flow should therefore vanish. A direct signature of this inconsistency is seen in figure 2: the coalescence velocity obtained from time-dependent numerical simulations (dashed lines) is significantly below the nondimensional velocity V_0 predicted from the similarity analysis (dotted line). This issue does not arise for inviscid lenses, for which the velocity profiles rapidly decay away from the bridge, and a perfect match with time-dependent simulations was found (Hack *et al.* 2020).

In this paper, we provide a detailed analysis of the coalescence of highly viscous lenses, and show that it is governed by a quasi-self-similar dynamics. The key result is that the coalescence velocity exhibits a slow relaxation, which in dimensionless variables reads

$$V \simeq V_0 + V_1(t), \quad \text{where} \quad V_1 \sim \frac{1}{\ln(t)}, \tag{1.1}$$

and $t \ll 1$ is the (dimensionless) time after coalescence. By performing a matched asymptotic analysis on the viscous thin-sheet equations, we will show that this slow relaxation of the velocity can be attributed to the long range of the velocity field, induced by the bridge but penetrating to the entire scale of the drop. This leads to an intricate coupling of the drop size and the neck region, and as a consequence, the local flow in the bridge is not strictly self-similar. The analysis is confirmed in detail by comparison to time-dependent numerical simulations of the thin-sheet equations, and accurately captures the slow convergence of the coalescence velocity (figure 2, solid line).

2. The viscous thin-sheet equations

Following the approach of Hack *et al.* (2020), the process of coalescence is modeled by the two-dimensional viscous thin-sheet equations (Erneux & Davis 1993; Ting & Keller 1990). The underlying approximations are the following: (i) Similar to sessile drops

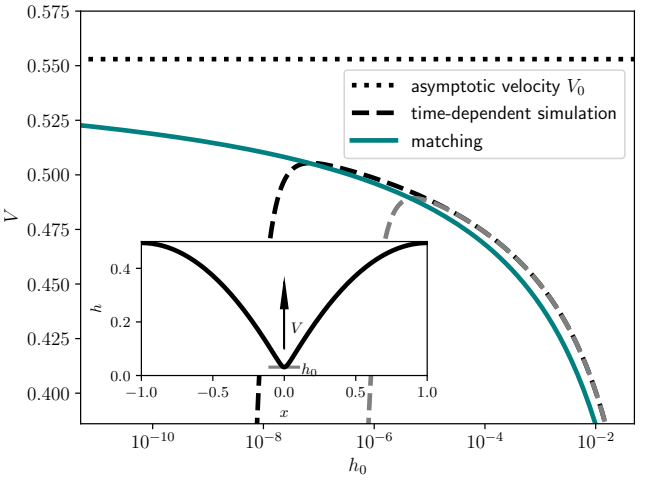

FIGURE 2. Coalescence velocity $V = dh_0/dt$ as a function of the local bridge height h_0 (see inset for definitions). Variables made dimensionless according to (2.3). Dashed lines are time-dependent numerical simulations, starting from two initial bridge heights (respectively near 10^{-8} and 10^{-6}); shortly after initialising, both simulations follow the same trend, where the coalescence velocity exhibits a slow convergence to the ultimate velocity V_0 (dotted). Solid line is the prediction (5.5) from the matched asymptotic analysis.

(Ristenpart *et al.* 2006; Hernández-Sánchez *et al.* 2012) the flow in the lenses is quasi-two-dimensional in the early stage of coalescence. (ii) The equilibrium contact angle θ is small, such that a slender body approximation can be employed. (iii) The influence of the bath on the dynamics is negligible, i.e., free slip boundary conditions can be employed at both interfaces of the 2D lenses. (iv) Due to negligible differences in surface tension between the bath and liquid lens and the liquid lens and air, the liquid lenses are assumed to be symmetrical with respect to the bath-air interface (asymmetric surface tensions can be mapped to an "effective" symmetric surface tension). The resulting model equations for negligible inertia of the flow, in dimensionless variables, take the form:

$$\frac{\partial h}{\partial t} + \frac{\partial}{\partial x}(hu) = 0, \tag{2.1}$$

$$h\frac{\partial^3 h}{\partial x^3} + 4\frac{\partial}{\partial x}\left(h\frac{\partial u}{\partial x}\right) = 0. \tag{2.2}$$

Here, $h(x,t)$ and $u(x,t)$, respectively, are the dimensionless interface height and the horizontal velocity. Dimensional variables $(\bar{x}, \bar{h}, \bar{u}, \bar{t})$ are scaled as

$$\bar{x} = Rx; \quad \bar{h} = 2\ell h = \theta R h; \quad \bar{u} = \frac{\gamma}{\eta}\theta u; \quad \bar{t} = \frac{R\eta}{\theta\gamma}t, \tag{2.3}$$

where R is the top view lens radius, ℓ the side-view lens height, with contact angle θ (cf. figure 1). The surface tension is denoted as γ and η is the viscosity of the liquid inside the lenses. The thin-sheet equations (2.1)-(2.2), respectively, correspond to mass and (horizontal) momentum conservation. The latter gives the balance between capillary forces (first term) and viscous forces (second term), while inertia was neglected.

We solve (2.1)-(2.2) numerically employing a finite element method implemented using

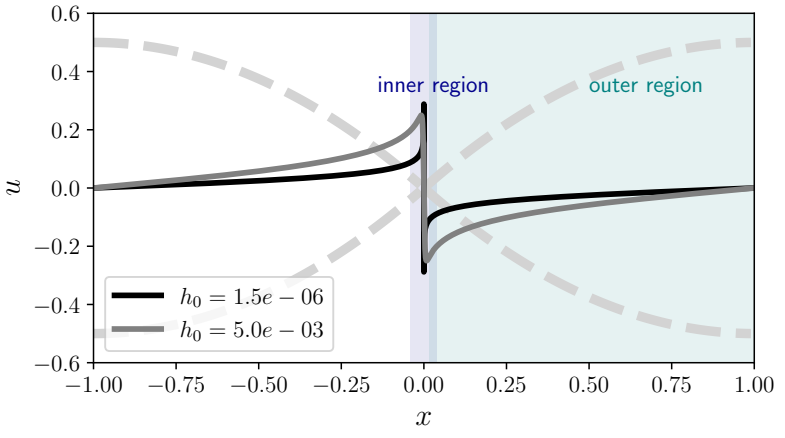

FIGURE 3. The velocity fields at early times of the coalescence process are not confined to the very narrow neck region at the center, but penetrate into the drops. The problem is analysed using a quasi-self-similar inner region and a nearly static outer region (colored patches for illustration, not to scale).

the library OOMPH-LIB (Heil & Hazel 2006). A spatially non-uniform mesh and a second order backward differentiation formula (BDF) scheme for the time stepping are used. In both the simulations and analysis, we assume that the lenses do not approach each other during the coalescence which allows us to model only half of the lenses (cf. dashed rectangle in figure 1) employing no-flux boundary conditions at the position of the lens apex. The simulations are initialized by two parabolas connected by an appropriate polynomial function at $|x| \ll 1$ such that $h_0(t = 0) = \mathcal{O}(10^{-6})$ or less.

Two exemplary snapshots of a time-dependent numerical simulation of the velocity field are shown as solid lines in figure 3. The initial drops are indicated as the grey dashed lines. Even at exceedingly small bridge heights h_0, i.e. at very early times of the coalescence process, the velocity field exhibits pronounced tails, that only slowly decay towards the lens apex. This means that the flow is not confined to the narrow bridge region, but penetrates far into the large-scale drop.

Based on this observation, we will analyse the problem in two distinct regions: (i) The outer region, where the drop profiles exhibit only small deviations from the equilibrium state, and (ii) the inner region corresponding to the connecting bridge, where surface tension drives the coalescence process, i.e., the growth of the bridge height h_0. Subsequently, the results of the two regions are matched, which will close the problem. Owing to symmetry, we restrict ourselves to $x > 0$ in the following.

3. The outer region

3.1. *Perturbation of static solution*

We start by seeking a solution for the outer region. Prior to the coalescence, we encounter a static drop without any flow. Indeed, (2.1)-(2.2) admit a static solution

$$h_s = \frac{1}{2}x(2 - x); \quad u_s = 0, \tag{3.1}$$

where the lens takes on a parabolic shape (ensuring the correct contact angle via $h_s'(0) = 1$). Once coalescence is initialized, at $t = 0$ and $x = 0$, a flow develops and penetrates into the drop. At large scales, this gives a disturbance with respect to (3.1), which is treated as a regular perturbation,

$$h(x,t) = h_s(x) + h_1(x,t); \quad u = u_1(x,t). \tag{3.2}$$

We do not know a priori how the perturbation grows over time, so for the time being we do not explicitly introduce a scale for h_1, u_1. However, it is understood that we assume $h_1 \ll h_s$ in the outer region, so that (2.1)-(2.2) can be expanded to

$$\frac{\partial h_1}{\partial t} + \frac{\partial}{\partial x}(h_s u_1) = 0, \tag{3.3}$$

$$h_s \frac{\partial^3 h_1}{\partial x^3} + 4\frac{\partial}{\partial x}\left(h_s \frac{\partial u_1}{\partial x}\right) = 0. \tag{3.4}$$

At this point two comments are in order with regards to the behaviour as $x \to 0$, for which the static profile $h_s \to 0$. First, the assumption $h_1 \ll h_s$ must break down in the proximity of $x = 0$; namely $h_s = 0$ at the drop edge but we are interested in describing a nonzero bridge height. Second, h_s multiplies the highest derivative in (3.4), which anticipates the appearance of a boundary layer as $h_s \to 0$. This boundary layer is the inner region depicted in figure 3, and must be analysed separately.

For now we proceed with the "outer" analysis, i.e. staying away from $x = 0$ and assuming the first term (surface tension) in (3.4) is sub-dominant with respect to the second term (viscosity). We can then integrate the equation twice to obtain

$$u_1(x,t) = C(t) \ln\left(\frac{x}{2-x}\right) + B(t), \tag{3.5}$$

where $C(t)$ determines the strength of the outer flow that remains to be determined. Using the boundary condition that $x = 1$ is a stagnation point, $u_1(1) = 0$, we find $B(t) = 0$. Inserting (3.5) into (3.3) gives after integration in time

$$h_1(x,t) = \tilde{C}(t)\left(x \ln\left(\frac{x}{2-x}\right) - \ln\left(\frac{x}{2-x}\right) - 1\right), \text{ where } \tilde{C}(t) = \int_0^t dt' C(t'). \tag{3.6}$$

Hence, we have found the spatial structure h_1, u_1 in the outer region. Importantly, the velocity u_1 diverges as $x \to 0$, which indeed needs to be regularised inside of a boundary layer. The remaining task is to compute the strength of the outer flow $C(t)$.

3.2. *Boundary layer scaling*

We now use the outer solution to establish the scalings of the boundary layer (the inner region). The boundary layer arises when the capillary term, $h_s \partial^3 h_1/\partial x^3$, becomes comparable to the viscous term in (3.4). Estimating the capillary and viscous terms from the outer solution h_1, u_1, we find the crossover distance

$$x \sim \frac{\tilde{C}(t)}{C(t)}. \tag{3.7}$$

To establish the time-dependence $C(t)$, we anticipate that in the crossover region the diverging outer velocity $u_1 \simeq C\ln(x)$ will be regularized by an inner solution, with $u_{\text{inner}} \sim \mathcal{O}(1)$. This then gives with (3.7):

$$C(t)\ln\left(\frac{C}{\tilde{C}}\right) \sim 1 \quad \Rightarrow \quad C(t) \sim \ln\left(\frac{C}{\tilde{C}}\right)^{-1} \underset{t\ll 1}{\sim} \frac{1}{-\ln(t)}, \tag{3.8}$$

where for the last step we have used the definition of $\tilde{C}$ in (3.6). Hence, the strength of the velocity in the outer region, $C(t)$, is arbitrarily small initially (as $t \to 0$), but increases in time. We obtain the boundary layer scalings

$$x \sim \frac{\tilde{C}(t)}{C(t)} \sim t, \quad h \sim t, \tag{3.9}$$

where for the scaling of h, we used that near the drop edge $h \sim x$. These estimations are useful in the analysis below, and will be verified a posteriori.

4. The inner region – manifold of quasi-similarity solutions

4.1. *Generalized similarity ansatz*

We now turn to the inner region. In Hack *et al.* (2020), we made a similarity ansatz assuming h, u near the bridge are perfectly self-similar. However, we have seen that a flow develops in the outer region, with a strength $C(t)$ that increases in time. It will turn out that this outer flow affects the inner region, so that the dynamics is not strictly self-similar. Therefore we propose the generalized similarity ansatz:

$$h(x,t) = h_0(t)\mathcal{H}(\xi, C); \quad u(x,t) = V(C)\mathcal{U}(\xi, C); \quad \xi = \frac{x}{h_0(t)}, \tag{4.1}$$

where the similarity profiles exhibit a weak time-dependence via $C(t)$. Inserting into (2.1)-(2.2) and using $V = \dot{h}_0$, one finds

$$\frac{h_0\dot{C}}{\dot{h}_0}\frac{\partial \mathcal{H}}{\partial C} + \mathcal{H} - \xi\mathcal{H}' + (\mathcal{H}\mathcal{U})' = 0, \tag{4.2}$$

$$\frac{4V}{\mathcal{H}}\left(\mathcal{H}\mathcal{U}'\right)' + \mathcal{H}''' = 0, \tag{4.3}$$

where a prime indicates a partial derivative with respect to ξ.

Now we see the importance of estimating the time dependence of $C(t)$, h_0 and $\dot{h}_0$. Namely, following the scaling in Sec. 3.2, it is clear that the first term in (4.2) vanishes as $t \to 0$. By consequence, the early-time similarity equations (4.2)-(4.3) reduce to

$$\mathcal{H} - \xi\mathcal{H}' + (\mathcal{H}\mathcal{U})' = 0, \tag{4.4}$$

$$\frac{4V}{\mathcal{H}}\left(\mathcal{H}\mathcal{U}'\right)' + \mathcal{H}''' = 0. \tag{4.5}$$

These equations only involve derivatives with respect to ξ, so that they can be solved as a set of ordinary differential equations. We remind that C still appears as a parameter through $V(C)$, which will be found by matching to the outer solution. In leading order however, a constant velocity $V = V_0$ implies $h_0 \sim t$ which is consistent with (3.9).

4.2. *Boundary conditions and asymptotics of the similarity solutions*

The remaining system (4.4)-(4.5) is fourth order, and contains an unknown parameter V. We thus need five boundary conditions to close the problem. At $\xi = 0$, we impose

$$\mathcal{H}(0) = 1; \quad \mathcal{H}'(0) = 0; \quad \mathcal{U}(0) = 0, \tag{4.6}$$

where the latter two stem from symmetry considerations. These boundary conditions admit a family of similarity solutions, with two examples shown in figure 4. To close the problem, two further boundary conditions for $\xi \to \infty$ need to be formulated, by matching to the outer solution. For this we consider the asymptotics of (4.4)-(4.5) as $\xi \to \infty$, i.e.

$$\mathcal{H} \sim A_0\xi + A_1 \ln(\xi) + A_2, \tag{4.7}$$

$$\mathcal{U} \sim -\frac{A_1}{A_0}\left(\ln(\xi) - 2\right) - A_2/A_0, \tag{4.8}$$

leaving us with three† degrees of freedom (A_0, A_1, A_2). The matching analysis will fix the two remaining boundary conditions, selecting the values of A_0 and A_1 (while A_2 then follows from solving the system of ODEs (4.4)-(4.5) with the boundary conditions (4.6)).

Importantly, the velocity $\mathcal{U}$ in (4.8) does not decay to zero at large distances ($\xi \gg 1$). The solution presented in Hack *et al.* (2020) is recovered by setting $A_0 = 1$, $A_1 = 0$, for which $\mathcal{U}$ approaches a constant value; this solution is shown as the dark solid line in figure 4. It will turn out that this is the "ultimate" similarity solution, which is approached as $t \to 0$. As we will see, however, matching the long-ranged flow inside the drop far from the bridge calls for $A_1 \neq 0$, so that the velocity field exhibits a logarithmic tail (figure 4, purple line). For the remaining steps it turns out convenient to work with an integral of (4.5),

$$\mathcal{H}\mathcal{H}'' - \frac{1}{2}\mathcal{H}'^2 + 4V\mathcal{H}\mathcal{U}' + \mathcal{K} = 0. \tag{4.9}$$

Here the constant $\mathcal{K} = -(\mathcal{H}''(0) - 4V)$ is related to A_1 by

$$A_1 = \frac{\mathcal{K} - \frac{1}{2}A_0^2}{4V} \tag{4.10}$$

and can thus be employed to control the outer asymptotics.

5. Matched asymptotics

5.1. *Slow convergence of the coalescence velocity*

Finally, we match the inner and outer solutions. This will offer the sought-after $C(t)$ and via $V(C)$ offers the time dependence of the coalescence velocity. Expanding the outer solution for $x \ll 1$ and the inner solution for $\xi \gg 1$, we obtain two overlapping representations:

$$h_{\text{outer}} \simeq x - \tilde{C}(\ln(2/x) - 1), \quad h_{\text{inner}} \simeq A_0 x + h_0 A_1 \ln\left(\frac{x}{h_0}\right) + h_0 A_2, \tag{5.1}$$

$$u_{\text{outer}} \simeq C \ln\left(\frac{x}{2}\right), \qquad u_{\text{inner}} \simeq V\left(-\frac{A_1}{A_0}\left(\ln\left(\frac{x}{2}\right) + \ln\left(\frac{2}{h_0 e^2}\right)\right) - \frac{A_2}{A_0}\right). \tag{5.2}$$

† Given that the system is fourth order, there should be a further degree of freedom as $\xi \to \infty$. However, it can be shown by perturbation analysis of (4.7)-(4.8) (cf. Eggers & Fontelos (2015)), that this degree of freedom appears as a prefactor of a term decaying through an exponential in ξ as long as $A_0 > 0$, which is always the case in this coalescence problem. The degree of freedom does thus not appear in our leading order asymptotics.

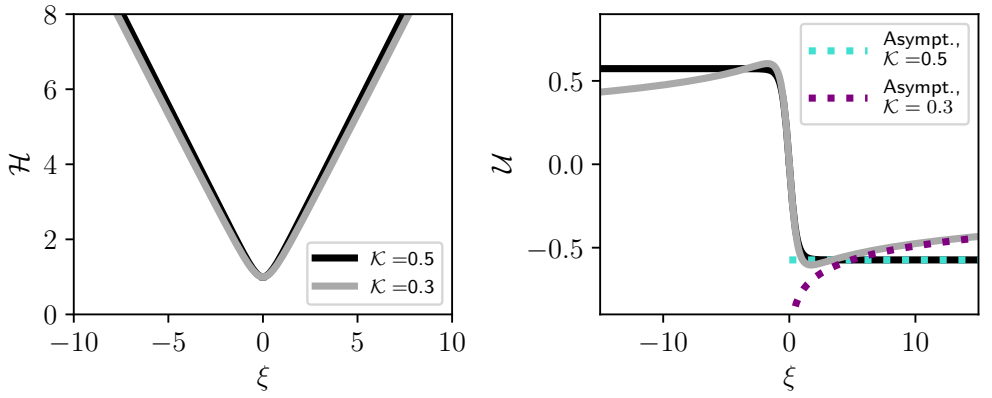

FIGURE 4. Similarity solutions calculated by numerically solving (4.4) and (4.9) with boundary conditions (4.6) and $\mathcal{H}'(\infty) = 1$ for two different values of $\mathcal{K}$. Dotted lines show large-ξ asymptotics (4.7) and (4.8).

Equating the leading order in h gives $A_0 = 1$. Matching the expansions in u then gives

$$C = -VA_1, \quad \text{and} \quad -A_1\left(\ln\left(\frac{2}{h_0}\right) - 2\right) = A_2, \tag{5.3}$$

which results in

$$C = \frac{VA_2}{\ln\left(\frac{2}{h_0}\right) - 2}. \tag{5.4}$$

Noting that $h_0 \sim t$, to leading order, we indeed find the anticipated (3.8).

We now translate these results, in particular (5.4), to the coalescence velocity $V = V_0 + V_1$ as announced in (1.1). First, we note that in the strict limit where $h_0 \to 0$, (5.4) implies that $C \to 0$ and thus $A_1 \to 0$. This boundary condition $A_1 = 0$, complemented by $A_0 = 1$ and (4.6), gives the ultimate similarity solution that is indicated by the dark solid lines in figure 4. We denote the corresponding values of V and A_2 as $V_0 = 0.553$ and $A_{2,0} = 0.573$, where V_0 is the ultimate coalescence velocity. Second, we consider the correction V_1 of the coalescence velocity that quantifies the slow convergence to V_0. Since this correction is due to the outer flow, we make the ansatz $V_1 = c_1 C$, where $c_1 = -2.5$ is determined numerically (see the numerical matching below). Inserting this together with $V = V_0 + V_1$ into (5.4) gives (for small h_0)

$$V_1 = \frac{c_1 A_{2,0} V_0}{\ln(\alpha/h_0)}, \qquad \text{with} \qquad \alpha = 2e^{-(2+c_1 A_{2,0})} = 1.1, \tag{5.5}$$

Hence, the correction to the coalescence velocity only evolves logarithmically with h_0. We remind that in dimensional terms, the slow convergence is associated to the ratio $\bar{h}_0/\ell$, where ℓ is the drop height. The velocity obtained from (5.5) is in good agreement with the results from time-dependent simulations as shown in figure 2 (solid line).

5.2. *Numerical matching*

Given that the expansion in h_0 involves logarithms, and thus converges very slowly, it worthwhile to numerically solve the matching conditions. This allows us to solve the quasi-self-similarity equations at finite h_0 with the matched boundary conditions

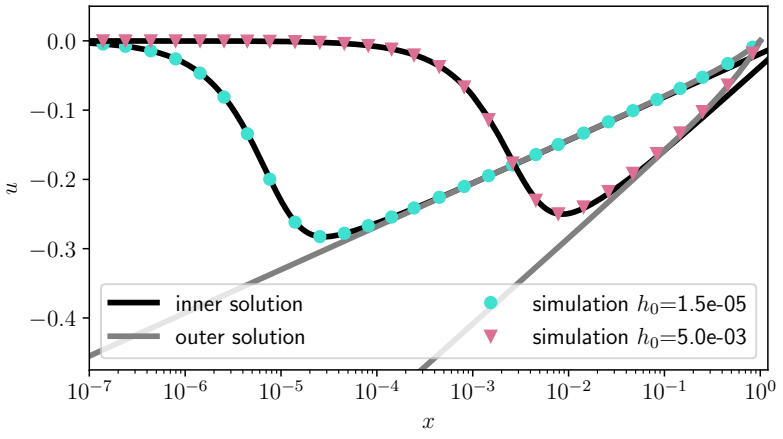

FIGURE 5. Two examples of the matching inner and outer solutions at given h_0, showing the excellent agreement with time-dependent simulations.

calculated without relying on the leading order approximations ($A_2 \approx A_{2,0}$, $V_1 \approx c_1 C$) made above. Together with (4.10), the condition (5.3) implies a h_0-dependent map $\mathcal{K}_{h_0}(V)$, which is obtained by numerically solving the following equation for $\mathcal{K}$:

$$\frac{\frac{1}{2} - \mathcal{K}}{4V} - A_2(V, \mathcal{K}) \left(\ln\left(\frac{2}{h_0}\right) - 2 \right)^{-1} = 0. \tag{5.6}$$

Here, $A_2(V, \mathcal{K})$ is obtained by numerically solving (4.4)-(4.9) at given $(V, \mathcal{K})$ as an initial value problem with (4.6) and $A_0 = 1$ as boundary conditions. For each value of h_0, the "missing" boundary condition is thus provided implicitly by the map $\mathcal{K}_{h_0}(V)$ resulting from (5.6). This map can be inserted in (4.9), allowing us to find a unique similarity solution associated to h_0. The thus computed inner and outer solutions are found to be in excellent agreement with full time-dependent simulations as exhibited in figure 5 for two different values of h_0. The symbols are snapshots from a time-dependent numerical simulation of (2.1)-(2.2), while the black and grey solid lines give the corresponding inner and outer solutions, respectively. From this procedure, we also get numerically the correction to the instantaneous velocity $V(h_0)$ which can be employed to compute the constant c_1 in (5.5). The numerically obtained $V_1(h_0)$ (not shown here) is in good agreement with the expression (5.5) and exhibits, as expected, a slightly better match with the time-dependent simulations at larger h_0.

6. Conclusion

In the present work, we have analysed the coalescence dynamics of viscous liquid lenses. We restricted ourselves to the case where the flow in the bath is negligible, which is a consistent approximation for lenses of high viscosity. The common scenario in coalescence, and pinch-off, is that the flow remains localised into the narrow neck region. However, it is found for viscous lenses that the velocity field develops long logarithmic tails that generate a flow inside the large-scale drops. A consequence of this flow is that the coalescence velocity is not constant, but exhibits corrections that depend logarithmically on the ratio $\bar{h}_0/\ell$, the neck size over the drop size. Only in the limiting case $\bar{h}_0/\ell \to 0$, i.e., for a perfect scale separation, one approaches a universal velocity of pinch-off. Here, we

analysed this scenario in full detail for the merging of two-dimensional drops, leading to slowly evolving similarity solutions, as is confirmed by direct numerical integrations of the thin-sheet equations.

Usually, a two-dimensional analysis of the coalescence is sufficient for sessile drops (and inertial liquid lenses), since in those cases the flow remains confined to the neck region. For the system discussed here, the extended logarithmic tails will make the problem sensitive to the flow in the large scale drops. Three-dimensional liquid lenses will exhibit a modified outer flow (3.5). The structure as presented here, however, is expected to be valid also in the three-dimensional case; only the numerical coefficients in (5.4) should be affected.

More generally, the dynamical structure of the problem bears a strong similarity with drop spreading, where the motion of the contact line also induces a weak flow on the scale of the drop (Bonn *et al.* 2009). The spreading velocity exhibits a logarithmic dependence on the scale separation between drop size and the characteristic scale of the contact line in that case too. An important difference, however, is that for drop spreading the inner problem retains a universal structure and is governed by a single similarity solution. Here we found that for viscous lens coalescence, the dynamics evolves along a family of similarity solutions. This resembles the description of the thin film flow between a settling sphere and a two phase boundary by Jones & Wilson (1978). We expect that a quasi-self-similar approach as presented here might be fruitful to a broader class of problems.

We are grateful to J. Eggers for discussions. W.T. acknowledges support by the European Unions Horizon 2020 research and innovation programme under the Marie Sklodowska-Curie grant agreement No 722497 - LubISS. M. A. H. acknowledges support from an Industrial Partnership Programme of the Netherlands Organisation for Scientific Research (NWO), cofinanced by Canon Production Printing Netherlands B.V., University of Twente, and Eindhoven University of Technology. C.D. and J.H.S. acknowledge support from NWO through VICI Grant No. 680-47-632.

Declaration of Interests: The authors report no conflict of interest.

REFERENCES

Aarts, D. G. A. L., Lekkerkerker, H. N. W., Guo, H., Wegdam, G. H. & Bonn, D. 2005 Hydrodynamics of droplet coalescence. *Phys. Rev. Lett.* **95**, 164503.

Anand, S., Paxson, A. T., Dhiman, R., Smith, J. D. & Varanasi, K. K. 2012 Enhanced condensation on lubricant-impregnated nanotextured surfaces. *ACS Nano* **6**, 10122–10129.

Billingham, J. & King, A. C. 2005 Surface-tension-driven flow outside a slender wedge with an application to the inviscid coalescence of drops. *J. Fluid Mech.* **533**, 193–221.

Bonn, D., Eggers, J., Indekeu, J., Meunier, J. & Rolley, E. 2009 Wetting and spreading. *Rev. Mod. Phys.* **81** (2), 739.

Burton, J. C. & Taborek, P. 2007 Role of dimensionality and axisymmetry in fluid pinch-off and coalescence. *Phys. Rev. Lett.* **98**, 224502.

Delabre, U. & Cazabat, A.-M. 2010 Coalescence driven by line tension in thin nematic films. *Phys. Rev. Lett.* **104**, 227801.

Duchemin, L., Eggers, J. & Josserand, C. 2003 Inviscid coalescence of drops. *J. Fluid Mech.* **487**, 167–178.

Eddi, A., Winkels, K. G. & Snoeijer, J. H. 2013 Influence of droplet geometry on the coalescence of low viscosity drops. *Phys. Rev. Lett.* **111**, 144502.

Eggers, J. & Fontelos, M. A. 2015 *Singularities: Formation, Structure, and Propagation*. Cambridge University Press.

Eggers, J., Lister, J. R. & Stone, H. A. 1999 Coalescence of liquid drops. *J. Fluid Mech.* **401**, 293–310.

Erneux, T. & Davis, S. H. 1993 Nonlinear rupture of free films. *Phys. Fluids A* **5**, 1117–1122.

de Gennes, P.-G., Brochard-Wyart, F. & Quéré, D. 2004 *Capillarity and Wetting Phenomena: Drops, Bubbles, Pearls, Waves*. Springer.

Hack, M. A., Costalonga, M., Segers, T., Karpitschka, S., Wijshoff, H. & Snoeijer, J. H. 2018 Printing wet-on-wet: Attraction and repulsion of drops on a viscous film. *Appl. Phys. Lett.* **113**, 183701.

Hack, M. A., Tewes, W., Xie, Q., Datt, C., Harth, K., Harting, J. & Snoeijer, J. H. 2020 Self-similar liquid lens coalescence. *Phys. Rev. Lett.* **124** (19), 194502.

Heil, Matthias & Hazel, Andrew L 2006 oomph-lib–an object-oriented multi-physics finite-element library. In *Fluid-structure interaction*, pp. 19–49. Springer.

Hernández-Sánchez, J. F., Lubbers, L. A., Eddi, A. & Snoeijer, J. H. 2012 Symmetric and asymmetric coalescence of drops on a substrate. *Phys. Rev. Lett.* **109**, 184502.

Jones, A.F. & Wilson, S.D.R. 1978 The film drainage problem in droplet coalescence. *J. Fluid Mech.* **87** (2), 263–288.

Kamp, J., Villwock, J. & Kraume, M. 2016 Drop coalescence in technical liquid/liquid applications: a review on experimental techniques and modeling approaches. *Rev. Chem. Eng.* **33**, 1–47.

Lee, M. W., Kang, D. K., Yoon, S. S. & Yarin, A. L. 2012 Coalescence of two drops on partially wettable substrates. *Langmuir* **28**, 3791–3798.

Narge, R. D., Beysens, D. A. & Pomeau, Y. 2008 Dynamics drying in the early-stage coalescence of droplets sitting on a plate. *Eur. Phys. Lett.* **81**, 46002.

Paulsen, J. D., Burton, J. C. & Nagel, S. R. 2011 Viscous to inertial crossover in liquid drop coalescence. *Phys. Rev. Lett.* **106**, 114501.

Ristenpart, W. D., McCalla, P. M., Roy, R. V. & Stone, H. A. 2006 Coalescence of spreading droplets on a wettable substrate. *Phys. Rev. Lett.* **97**, 064501.

Shaw, J. M. 2003 A microscopic view of oil slick break-up and emulsion formation in breaking waves. *Spill Sci. Technol. Bull.* **8**, 491–501.

Smith, J. D., Dhiman, R., Anand, S., Reza-Garduno, E., Cohen, R. E., McKinley, G. H. & Varanasi, K. K. 2013 Droplet mobility on lubricant-impregnated surfaces. *Soft Matter* **9**, 1772–1780.

Thoroddsen, S. T., Qian, B., Etoh, T. G. & Takehara, K. 2007 The initial coalescence of miscible drops. *Phys. Fluids* **19**, 072110.

Ting, L. & Keller, J. B. 1990 Slender jets and thin sheets with surface tension. *SIAM J. Appl. Math.* **50**, 1533–1546.